Prestrain-induced bistability in the design of tensegrity units for mechanical metamaterials

Andrea Micheletti,[1] Filipe A. dos Santos,[2] and Simon D. Guest[3]
[1)] *Department of Civil and Computer Science Engineering, University of Rome Tor Vergata, via Politecnico 1, 00133, Rome, Italy*
[2)] *CERIS-NOVA, Department of Civil Engineering, NOVA School of Science and Technology, NOVA University of Lisbon, Quinta da Torre, 2829- 516 Caparica, Portugal*
[3)] *Department of Engineering, University of Cambridge, Trumpington Street, Cambridge CB2 1PZ, UK*

(*Electronic mail: micheletti@ing.uniroma2.it)

(Dated: 16 August 2023)

ABSTRACT

Tensegrity metamaterials are a type of artificial materials which can exploit the tunable nonlinear mechanical behavior of the constituent tensegrity units. Here we present reduced-order analytical models which describe the prestrain-induced bistable effect of two particular tensegrity units. Closed-form expressions of the critical prestrain at which a unit transitions into a bistable regime are derived. Such expressions depends only on the geometry of the units. The predictions of the reduced-order model are verified by numerical simulations and by the realization of physical models. The present results can be generalized to analogous units with polygonal base, and the proposed tensegrity units can be assembled together to form one-dimensional metamaterials with tailorable nonlinear features, such as multistability and solitary wave propagation.

Architected metamaterials have been studied extensively in recent years[1,2], with particular attention to multistable metamaterials obtained by tessellating units with bistable behavior. For instance, multistable metamaterials were proposed for energy trapping and impact mitigation[3], and for the stable transmission of mechanical signals over arbitrary distances[4]. The propagation of transition waves in one-dimensional lattices composed of concentrated masses and bistable springs was treated analytically[5], and typical multistable metamaterials were optimized[6] and extended to two and three dimensions[7].

In the particular class of tensegrity metamaterials the repeating unit is a tensegrity structure[8–10], that is, a prestressed cable-bar framework. Because many tensegrity structures are deployable and/or possess a highly nonlinear response depending on their geometry and level of prestress[11–13], these types of structures became of interest for realizing adaptive and tunable structures[14]. Researchers have used stimulus-responsive polymers to achieve programmable deployment of tensegrity structures[15], and studied the bandgap tuning of tensegrity chains numerically[16] and experimentally[17]. Tensegrity chains can also support the propagation of solitary waves, which was observed in one-, two-, and three-dimensional tessellations of tensegrity units[18–22]. The mechanical response of three-dimensional tensegrity metamaterials was studied with continuum models[23,24], and different regimes of wave propagations were shown to depend on the selfstress level[25]. In addition, optimal-density[26] and energy-dissipation[27] planar tensegrity metamaterials were proposed, and a systematic approach to obtain tensegrity metamaterials with desired properties was devised[28]. Although additively manufactured tensegrity-like metamaterials with no prestress have been experimentally studied[29–32], the additive manufacturing of prestressed tensegrity-like metamaterials has not been attempted yet. Nevertheless, possible prestressing procedures at the microscale could rely on 4D printing[33], for example by using two-photon laser printing of photo-responsive structures[34].

Here we introduce two tensegrity structures, the "six-node" and the "eight-node" units, which demonstrate a monostable-to-bistable transition triggered by changes in geometry and selfstress level. Previous research has shown that some tensegrity structures can exhibit bistable[35,36] or multistable[37] behavior. Our units are the smallest known spatial tensegrity structures with such features. Each unit show different aspects of the possible bistable regimes, with the six-node unit having no infinitesimal mechanisms, and the eight-node having three. We developed analytical models for each structure to calculate the *critical prestrain*, the amount of prestrain necessary for the units to enter a bistable regime. These models were consistent with the structures' symmetry properties and allowed us to derive closed-form expressions for the critical prestrain. We performed numerical simulations on one-dimensional assemblies of the units, which confirmed the expected prestrain-induced multistable behavior. We verified our analytical and numerical results through physical models with different bistable responses. These findings have implications for the design and benchmarking of mechanical metamaterials with adjustable multistable behavior.

A tensegrity structure $\mathscr{T}$ is given by a set of nodes, a set of edges, and a set of labels. The nodes are points in three-dimensional space, with position vector $\mathbf{p}_i$ for the i-th node and $\mathbb{p}$ denoting the collection of all nodal position vectors, while the edges connect pairs of nodes and are labeled as "bar" or "cable". The current length, rest length, and spring constant of the edge ij connecting nodes i and j are $l_{ij} = |\mathbf{p}_i - \mathbf{p}_j|$, $\bar{l}_{ij} > 0$, $k_{ij} > 0$, respectively. We consider an elastic energy[38]

$$U(\mathbb{p}) = \frac{1}{2}\sum_{ij\in\mathscr{E}} k_{ij}\,(l_{ij}(\mathbb{p}) - \bar{l}_{ij})^2\,. \tag{1}$$

At a selfstressed equilibrium configuration $\mathbb{p}^{(\mathrm{eq})}$ for $\mathscr{T}$, the elastic energy is stationary:

$$\partial_{\mathbb{p}} U(\mathbb{p}^{(eq)}) = \sum_{ij\in\mathscr{E}} t_{ij}\, \partial_{\mathbb{p}} l_{ij}\,(\mathbb{p}^{(\mathrm{eq})}) = \mathbf{A}(\mathbb{p}^{(\mathrm{eq})})\,\mathbf{t} = \mathbf{0}\,. \tag{2}$$

In (2), $\partial_{\mathbb{p}}(\cdot)$ denotes the derivative with respect to $\mathbb{p}$, while $t_{ij} = k_{ij}\,(l_{ij}(\mathbb{p}) - \bar{l}_{ij})$ is the axial force carried by an edge, linear in the edge elongation. The vector containing all axial forces is $\mathbf{t}$, and $\mathbf{A}$ is the *equilibrium operator*. The stationary condition (2) requires that the selfstress state $\mathbf{t}$ belongs to the nullspace of $\mathbf{A}(\mathbb{p}^{(\mathrm{eq})})$.

The *tangent stiffness operator*, $\mathbf{K}_T$, equal to the Hessian of the elastic energy, $\partial^2_{\mathbb{p}} U$, is

$$\mathbf{K}_T = \partial^2_{\mathbb{p}} U = \sum_{ij\in\mathscr{E}} \big(k_{ij}\,\partial_{\mathbb{p}} l_{ij} \otimes \partial_{\mathbb{p}} l_{ij} + t_{ij}\,\partial^2_{\mathbb{p}} l_{ij}\big) = \mathbf{K}_M + \mathbf{K}_G\,, \tag{3}$$

where the first and second terms in the summations contribute respectively to the *material stiffness operator*, $\mathbf{K}_M$, which depends on the spring constants, and the *geometric stiffness operator*, $\mathbf{K}_G$, which depends on the axial forces (see[36,39,40] for details). We recall that the *internal mechanisms* of $\mathscr{T}$, if any, are the sets of nodal displacements which do not cause first-order changes of the edge lengths[41,42], excluding rigid-body motions. Internal mechanisms and rigid-body motions lie in the nullspace of $\mathbf{K}_M$.

The positive definiteness of $\mathbf{K}_T$ is a sufficient condition for the stability of an equilibrium configuration; however, there are two more specialized stability conditions for tensegrity structures. The notion of *prestress stability*[43] applies to tensegrity structures with non-null self-stress possessing internal mechanisms. A tensegrity structure is said to be prestress stable if, for every internal mechanism $\mathbf{v} \in \mathrm{null}(\mathbf{K}_M)$,

$$\mathbf{K}_G\,\mathbf{v}\cdot\mathbf{v} > 0\,. \tag{4}$$

This condition states that every internal mechanism is associated to a first-order increase of the elastic energy, or, in other words, that the selfstress state stiffens every internal mechanisms. If (4) holds at a certain equilibrium configuration, and $\mathbf{K}_G$ has no negative eigenvalues, then we speak of *super stability*[44], that is, the structure at $\mathbb{p}^{(\mathrm{eq})}$ is stable independently of material properties and of the level of self-stress. On the contrary, if $\mathbf{K}_G$ has negative eigenvalues, whether there are internal mechanisms or not, then it is possible that a stable tensegrity structure at a certain selfstress level becomes unstable at larger selfstress levels[36,40]. In fact, given a selfstressed equilibrium configuration where $\mathbf{K}_T$ is positive definite and $\mathbf{K}_G$ has a negative eigenvalue, since $\mathbf{K}_G$ is linear in the axial forces t_{ij}, it is possible to scale up $\mathbf{K}_G$ with the selfstress in the elements by suitable changes of rest lengths until $\mathbf{K}_T$ is not positive definite anymore. Similar situations in which the (positive) material stiffness is in competition with a negative geometric stiffness occur also in typical continuum mechanics problems, such as, e.g., the buckling of a beam subjected to axial compression, the buckling of thin-walled columns with residual stresses, or the zero stiffness of prestressed rings obtained by bending a initially straight rod with circular cross section with respect to eversion deformations[45].

The case of a $\mathbf{K}_G$ with some negative eigenvalues applies to the two tensegrity units we propose: both are stable in a certain configuration at low to moderate self-stress levels but become unstable when the self-stress level exceeds a certain critical value. This leads to the emergence of two additional stable configurations, indicating a switch from a single- to a double-well energy landscape. The eight-node unit features also another bistable regime when its configuration is prestress unstable ($\mathbf{K}_G\,\mathbf{v}\cdot\mathbf{v} < 0$ for some $\mathbf{v} \in \mathrm{null}(\mathbf{K}_M)$). In the following, self-stress levels are quantified in a dimensionless way in terms of elements' *prestrain*, here defined as[40] $\varepsilon_0 := (\lambda_0 - \overline{\lambda})/\lambda_0$, with $\overline{\lambda}$ and λ_0 respectively the rest length of a characteristic element and its length in a reference equilibrium configuration.

Figure 1(a,b) depicts stable configurations for the six-node (a) and the eight-node unit (b), corresponding to different prestrain values. The six-node unit has no internal mechanisms, while the eight-node unit has three internal mechanisms and is prestress-stable when its geometric parameters range in a certain set. Each unit can exhibit configurations with symmetry point group D_{2h} (left configurations in Fig.1(a,b)) and with symmetry point group D_2 (right configurations in Fig.1(a,b)). In the former case, symmetry operations correspond to an inversion center, three mirror planes, and three two-fold cyclic-symmetry axes, while in the latter case, they correspond to just three two-fold cyclic-symmetry axes.

By performing numerical simulations based on the full-order model described above, we found that the structures depicted on the left in Fig.1(a) and (b) become bistable when the prestrain of elastic cables exceeds a certain critical value. By chosing a D_{2h} symmetric configuration as reference configuration, the bars were considered rigid, while the cables were modeled as elastic springs with same spring constant k, rest length $\overline{\lambda}$, and prestrain ε_0, except for the two vertical cables in the eight-node unit shown in Fig.1(b, left), which were modeled as inextensible. To enforce rigidity and inextensibility constraints, the corresponding members were assigned a large spring constant relative to k. With these choices, the equilibrium condition (2) is satisfied in the reference configuration. The smallest nonzero eigenvalue ξ of $\mathbf{K}_T$ is then computed as a function of prestrain in that configuration. The results are shown in Fig.1(c,d) and reveal that the smallest nonzero eigenvalue becomes negative when prestrain values become large enough. We observed that the associated eigenvector corresponds to a twisting deformation mode with D_2 symmetry (Fig.1(e,f)). Afterward, we run a number of simulations in which the D_{2h} reference configurations shown in Fig.1(a) and (b) are perturbed by random nodal displacements of small magnitude, with no prescribed symmetry, and the energy (1) is minimized by using a standard numerical procedure. For the same values of prestrain determined by the analysis of $\mathbf{K}_T$ in the reference configuration, when the prestrain ε_0 is small, the structures return to the unperturbed D_{2h} symmetric configuration, while for large prestrains, they find either one of two other stable equilibrium configurations, away from the unperturbed one, both possessing D_2 symmetry and mirror images of each other. The stability of each of the D_2 symmetric equilibrium configuration is verified by the positive definiteness

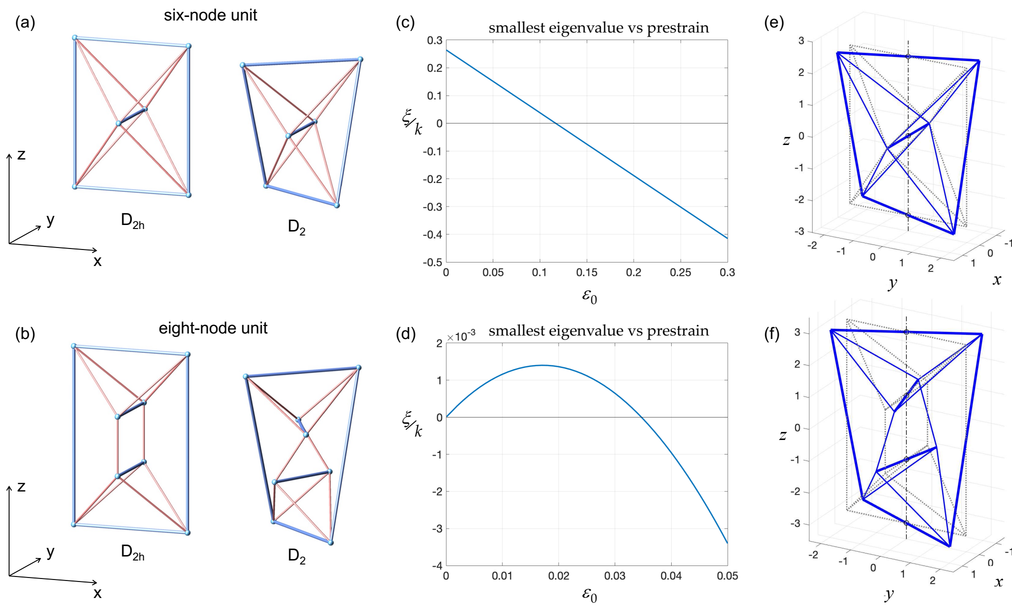

FIG. 1. The "six-node" (a) and the "eight-node" (b) units, both shown in equilibrium configurations with D_{2h} and D_2 symmetry. Normalized smallest nonzero eigenvalue of the tangent stiffness matrix vs. prestrain (c,d) and corresponding eigenmodes (e,f): for the six-node unit, with geometric parameters (see Fig.2(a)): $c/a = 10/8$, $b/a = 5/8$ (c,e); for the eight-node unit, with geometric parameters (see Fig.3(a)): $c/a = 12/8$, $b/a = 5/8$, $d/a = 4/8$ (d,f).

of $\mathbf{K}_T$. No other equilibrium configurations were found in the vicinity of the reference configuration, thus demonstrating the prestrain-induced monostable to bistable transition of the units. The admissibility of axial forces, i.e., cables being in tension, is checked a posteriori in all calculations.

We describe next the two reduced-order models of these units. Consider the six-node unit in the reference configuration defined by the parameters a, b, and c shown in Fig.2(a), consisting of rigid bars and linear springs (the cables). The springs are assumed to have the same spring constant k, and their rest length is $\lambda_N \leq \lambda_0 = \sqrt{a^2+b^2+c^2}$. The system's D_2 symmetric configurations can be identified by the relative rotation angle 2θ about the vertical axis between the bars AB and CD. In the projected view on the $x-y$ plane (Fig.2(b)), the bar EF remains orthogonal to the line bisecting the angle 2θ. Springs can be grouped in two categories: those whose length increase with θ, and those whose length decrease with θ, depicted respectively in orange and green in Fig.2(a).

The elastic energy of the system is given by

$$U(\theta) = 2k\Big((\lambda_1(\theta)-\overline{\lambda})^2 + (\lambda_2(\theta)-\overline{\lambda})^2\Big), \tag{5}$$

with λ_1 and λ_2 the current lengths of the orange and green springs, respectively. The Supplementary Material includes calculations demonstrating that the energy is stationary at $\theta = 0$, and the corresponding configuration is stable only when the prestrain ε_0 is less than a critical value $\varepsilon_{\mathrm{crit}}$, which is determined solely by the geometry and can be expressed as

$$\varepsilon_{\mathrm{crit}} = \frac{1}{1+\dfrac{1}{\sin^2\alpha}}, \tag{6}$$

with $\alpha = \frac{1}{2}\widehat{EAF}$. Fig.2(c) shows the monotonic relationship between α and $\varepsilon_{\mathrm{crit}}$. Fig.2(d) displays the change in elastic energy from the value U_0 in the reference configuration, normalized by k, λ_0^2, for different prestrains, and highlights the shift from a monostable to a bistable regime as prestrain increases, along with the ranges in which axial forces in cables are positive.

We consider now the eight-node unit in the reference configuration defined by the parameters a, b, c, and $d < c$ shown in Fig.3(a), obtained from the previous structure by doubling the central bar and adding two vertical cables. We assume that bars are rigid and that cables have same spring constant k and rest length $\overline{\lambda} < \lambda_0 = \sqrt{a^2+b^2+(c-d)^2}$, except for EG and FH, which are inextensible. We require the structure to retain D_2 symmetry during a motion. Therefore, if AB rotates with respect to CD by an angle $2\theta_1$ about the z axis, and EF rotates with respect to GH by an angle $2\theta_2$ about the same axis, then in the projected view onto the Cartesian $x-y$ plane

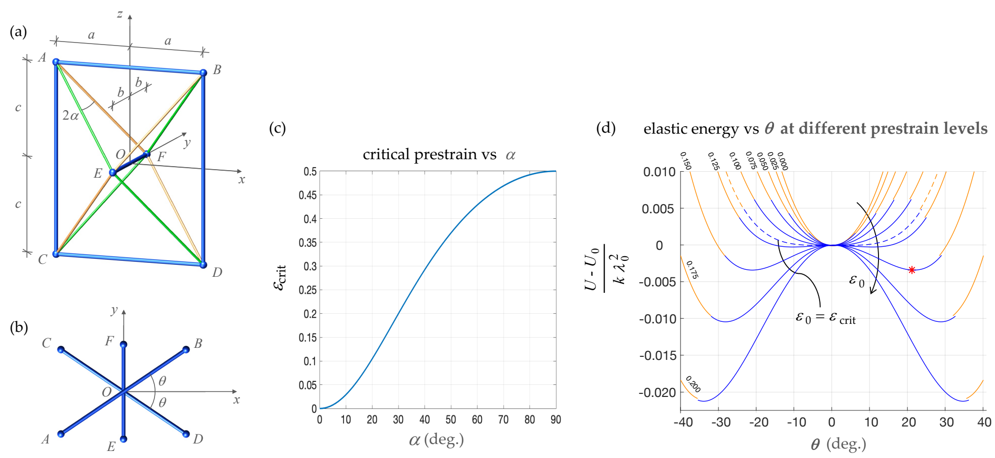

FIG. 2. The six-node tensegrity unit: (a) at the configuration with D_{2h} symmetry, axonometric view; (b) at a configuration with D_2 symmetry, projection onto the x-y plane with only bars AB, CD, and EF shown. (c) Critical prestrain $\varepsilon_{\text{crit}}$ vs $\alpha = \frac{1}{2}\widehat{EAF}$ for the six-node unit. (d) Plot of the non-dimensional change of elastic energy from the value U_0 in the reference configuration for various values of prestrain for the six-node unit with $c/a = 10/8$, $b/a = 5/8$. The blue color of the curves indicates that cables axial forces are positive, the orange color that some cables have negative axial forces. The dashed curve represents the energy corresponding to the critical prestrain ($\varepsilon_{\textbf{crit}} = 0.117$). The starred point corresponds to the equilibrium configuration shown in Fig.1(a, right) as obtained from the full-order model.

the bisecting lines of these angles remains orthogonal to each other (Fig.3(b)). As in the previous model, there are two kind of springs, depicted in Fig.3(a) in orange, with length λ_1, and green, with length λ_2. The angles θ_1 and θ_2 are the two Lagrangian parameters for the system.

The elastic energy is given by

$$U(\theta_1,\theta_2) = 2k\Big((\lambda_1-\overline{\lambda})^2 + (\lambda_2-\overline{\lambda})^2\Big). \tag{7}$$

Calculations given in the Supplementary Material show that $(\theta_1,\theta_2) = (0,0)$ is an equilibrium configuration, and that the corresponding geometric and material stiffness operators can be expressed as

$$[\mathbf{K}_G] = 8k\frac{\lambda_0-\overline{\lambda}}{\lambda_0}\begin{bmatrix} -\frac{a^2}{c}(c-d) - \frac{a^2b^2}{\lambda_0^2} & \frac{a^2b^2}{\lambda_0^2} \\ \frac{a^2b^2}{\lambda_0^2} & \frac{b^2}{d}(c-d) - \frac{a^2b^2}{\lambda_0^2} \end{bmatrix},$$

and

$$[\mathbf{K}_M] = 8k\frac{a^2b^2}{\lambda_0}\begin{bmatrix} 1 & -1 \\ -1 & 1 \end{bmatrix}.$$

Internal mechanisms consistent with the D_2 symmetry have the form

$$[\mathbf{v}] = \bar{\theta}\begin{bmatrix} 1 \\ 1 \end{bmatrix}, \tag{8}$$

with $\bar{\theta}$ an arbitrary scalar, and correspond to the relative rigid rotations of the tetrahedron $ABEF$ with respect to the tetrahedron $CDGH$ about the vertical symmetry axis.

The prestress stability condition, $\mathbf{K}_G\,\mathbf{v}\cdot\mathbf{v} > 0$ gives

$$8\,k\,\varepsilon_0(c-d)\Big(-\frac{a^2}{c}+\frac{b^2}{d}\Big) > 0, \tag{9}$$

where $\varepsilon_0 = (\lambda_0 - \overline{\lambda})/\lambda_0$. Since $c > d$, we have

$$\frac{b^2}{d} > \frac{a^2}{c}, \tag{10}$$

or, by introducing the dimensionless parameters

$$\delta := \frac{b}{a}, \qquad \gamma := \frac{d}{c}, \tag{11}$$

we can rewrite the *prestress stability condition* as

$$\gamma < \delta^2. \tag{12}$$

By considering that $\varepsilon_0 > 0$, the condition for positive definiteness of $\mathbf{K}_T = \mathbf{K}_M + \mathbf{K}_G$ amounts to requiring that

$$-\varepsilon_0\left(\frac{c-d}{c\,d} + \frac{1}{\lambda_0^2}\left(\frac{b^2}{d} - \frac{a^2}{c}\right)\right) + \frac{1}{\lambda_0^2}\left(\frac{b^2}{d} - \frac{a^2}{c}\right) > 0, \tag{13}$$

or,

$$\varepsilon_0 < \frac{1}{1 + \dfrac{1-\gamma}{1-\dfrac{\gamma}{\delta^2}}\dfrac{1}{\sin^2\alpha}} =: \varepsilon_{\textbf{crit}}, \tag{14}$$

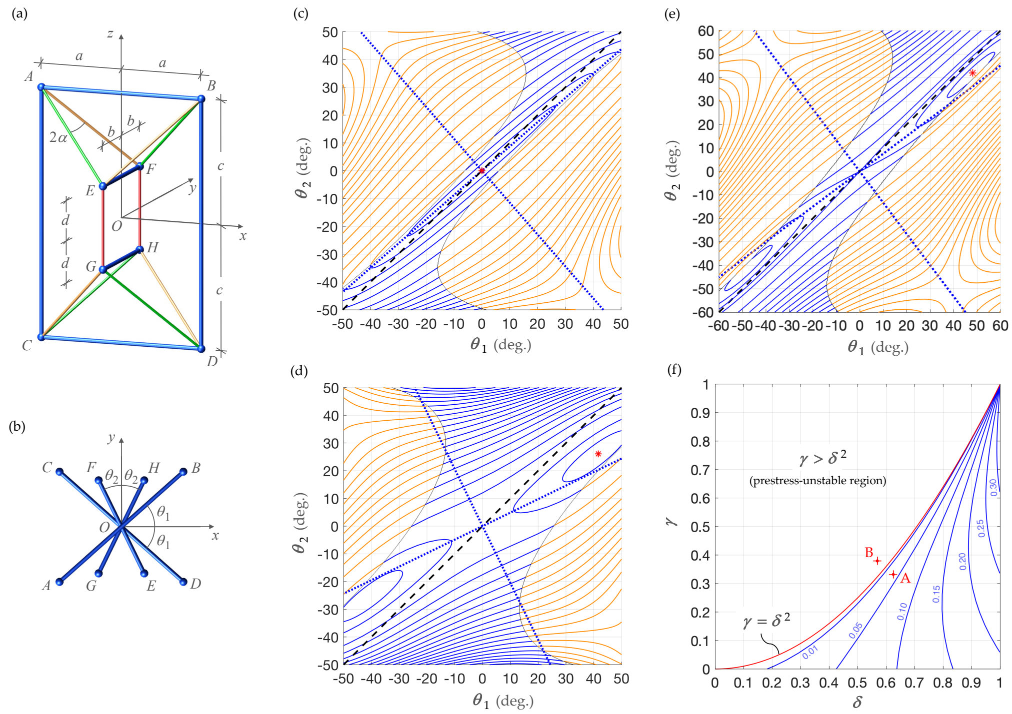

FIG. 3. The eight-node tensegrity unit: (a) at the configuration with D_{2h} symmetry, axonometric view; (b) at a configuration with D_2 symmetry, projection onto the x-y plane with only bars AB, CD, EF, and GH shown. (c,d) Contour plots of the elastic energy for the prestress-stable eight-node unit A, with $\delta := b/a = 5/8$ and $\gamma := d/c = 1/3$, which give $\alpha = 23.84°$ and $\varepsilon_{\mathbf{crit}} = 0.0347$, for a prestrain below, $\varepsilon_0 = 0.0300$ (c), and above, $\varepsilon_0 = 0.1500$ (d), the critical value. Blue contour lines indicate that cables axial forces are positive, orange contour lines that some cables have negative axial forces. The dotted lines are parallel to the eigenvectors, while the dashed line corresponds to the direction of the internal mechanism ($\theta_1 = \theta_2$), evaluated at $(\theta_1, \theta_2) = (0,0)$. The starred points represent stable equilibrium configurations obtained numerically from the full-order model. (e) Contour plots of the elastic energy for the prestress-unstable eight-node unit B, with $\delta := b/a = 8/14$ and $\gamma := d/c = 8/21$, which gives $\alpha = 22.72°$, for the prestress strain $\varepsilon_0 = 0.0700$. (f) Contour plot of the critical prestrain for the eight-node unit with $c/a = 3/2$, as a function of $\delta := b/a$ and $\gamma := d/c$. The two configurations, eight-node A, with $\delta = 5/8$, $\gamma = 1/3$, and eight-node B, with $\delta = 8/14$, $\gamma = 8/21$, are marked.

where $\sin\alpha = b/\lambda_0$, with $\alpha = \frac{1}{2}\widehat{EAF}$. Notice that, in the limit for $d \to 0$, $\gamma \to 0$, and we find (6) again, while, if $b \to 0$, then

$$\varepsilon_{\mathbf{crit}} \to \frac{1}{1 + (1-\gamma^{-1})\dfrac{\lambda_0^2}{a^2}}\,. \tag{15}$$

Moreover, we have that $\varepsilon_{\mathbf{crit}} \to 0$ when $\gamma - \delta^2 \to 0$.

Figure 3(c,d) shows the contour plots of the elastic energy $U(\theta_1, \theta_2)$ for a prestress stable eight-node unit (A), for prestrain values above (c) and below (d) the critical value. The plots display also the region with positive axial forces in cables, the mechanism and eigenvector directions at $(\theta_1, \theta_2) = (0,0)$, and the stable configurations obtained numerically using the full-order model. It can be observed that, for the monostable structure, the mechanism direction is close to one of the eigenvector directions. Fig.3(e) displays the contour plot of the energy for a prestress-unstable eight-node unit (B). Stable configurations for this unit are located in the direction of the mechanism. Fig.3(f) shows the contour plot of the critical prestrain (14) for $c/a = 12/8$, with the marked positions defining units eight-node A and eight-node B.

One-dimensional assemblies of each unit were analyzed numerically using the full-order model. Adjacent units in an assembly share a subset of elements, as shown in Fig.4(a,b). Bars are rigid and cables linearly elastic, except for the cables parallel to the longitudinal axis, which are inextensible. In order to have equal units in geometry and selfstress, we considered $a = b$, and same prestrain ε_0 and spring constant k for all elastic cables, except for the four cables at each end of the assembly, which have spring constant $k/2$.

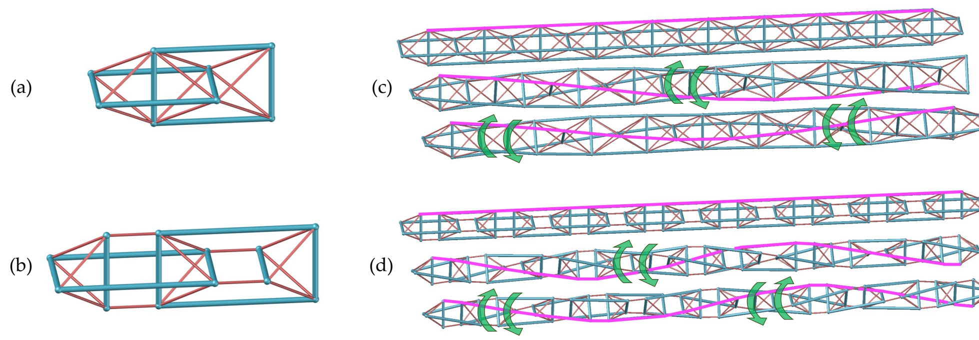

FIG. 4. Two-unit assemblies, based on the six-node (a) and eight-node (b) tensegrity units. (c) Multiple stable equilibrium configurations of a chain assembled from the six-node unit ($c/a = 1.5$, $b/a = 1$, giving $\alpha = 29.02^\circ$, $\varepsilon_{\mathbf{crit}} = 0.1905$). The straight configuration is obtained for $\varepsilon_0 = 0.1$; two different twisted configurations are obtained for $\varepsilon_0 = 0.2$. (d) Multiple stable equilibrium configurations of a chain assembled from the eight-node unit ($c/a = 2$, $\delta = 1$, $\gamma = 1/3$ giving $\alpha = 30.96^\circ$, $\varepsilon_{\mathbf{crit}} = 0.2093$). The straight configuration is obtained for $\varepsilon_0 = 0.15$; two different twisted configurations are obtained for $\varepsilon_0 = 0.26$. In each case, a longitudinal row of elements is highlighted. The curved arrow pairs indicate the twisting direction of the units.

TABLE I. Geometric characterization of the realized tensegrity units.

	six-node unit		eight-node case A (prestress-stable)		eight-node case B (prestress-unstable)
	monostable	bistable	monostable	bistable	bistable
a [mm]	135	135	135	135	135
b [mm]	62	62	130	130	80
c [mm]	170	170	235	235	235
d [mm]	-	-	85	85	85
λ_0 [mm]	226	226	240	240	217
ε_{crit} [%]	7.0	7.0	21.9	21.9	-
$\overline{\lambda}$ [mm]	212	190	190	160	200
ε_0 [%]	6.2	15.9	20.8	33.3	7.8

Starting from prestressed assembly configurations with D_{2h} symmetric units, simulations are conducted in two steps. First, a twisting load is applied to the assembly, and the equilibrium configuration reached under such load is determined. Second, the twisting load is removed, and the final equilibrium configuration is determined. If $\varepsilon_0 < \varepsilon_{\mathrm{crit}}$, the final equilibrium configuration coincides with the starting configuration. If $\varepsilon_0 > \varepsilon_{\mathrm{crit}}$, different twisted equilibrium configurations are obtained depending on the applied and removed twisting load, demonstrating the multistable response of such assemblies. Figure 4(c,d) shows simulation results for particular assemblies of both types of units. All units are twisted in the same way in Figure 4(c,d,middle) in a periodic overall deformation, while in Figure 4(c,d,bottom) the assembly is twisted partly in one way and partly in the other way.

Physical models of the two units are presented next. The units were built of wooden bars and additively manufactured nodes and cables obtained by fused deposition modeling. Cables were fabricated using polyurethane, except for the two 'inextensible cables' in the eight-node unit, which were realized in polylactic acid. To connect the bars and cables that converge into the nodes of the units, specially designed universal joints realized in polylactic acid were used. Five tensegrity units with different prestrain were tested to confirm the monostable to bistable transition, two specimens of the six-node unit with monostable and bistable configurations, and three specimen of the eight-node unit: case A, prestress-stable, which can be either monostable or bistable, and case B, which is prestress-unstable and bistable. Dimensions and prestrain of the units are listed in Table I. Small random perturbations of the equilibrium configurations were manually applied to verify the expected monostable/bistable behavior. Photos of the units are shown in Fig.5(a-f). Additionally, Fig.5(g-j) depicts models of three-unit and nine-unit tensegrity chains based on the six-node unit.

This study can be extended to similar units with a polygonal base (see the Supplementary Material) and has potential applications to the design and benchmarking of multistable metamaterials. Future work can regard the additive manufacturing of tensegrity-like structures with cables replaced by bars, using compliant hinges instead of pin-connections[30], and employing responsive materials, such as photo-thermal-

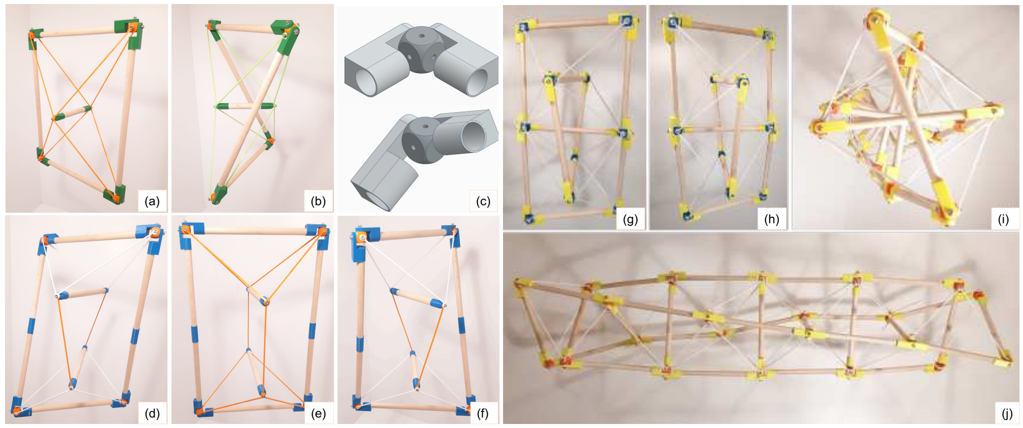

FIG. 5. Photos of the models of the two tensegrity units (a-f). Six-node tensegrity unit: monostable (a) and bistable (b). Detail of the universal joint (c). Eight-node tensegrity unit: bistable (case A) (d), monostable (case A) (e), bistable (case B) (f). Photos of models of two tensegrity chains based on the six-node tensegrity unit (g-j). A three-unit bistable structure showing two stable configurations (a,b). A nine-unit structure in one of its stable configurations, shown in a top (c) and lateral (d) view.

responsive liquid-crystal elastomers[34,46], that have actuation strains up to about 0.2[47]. The effect of external loads, nodal constraints, and more elaborate constitutive models could also be explored for better predictions of monostable-bistable switching.

See the Supplementary Material for detailed calculations on the six-node and eight-node units.

AM's work was supported by the Italian Minister of University and Research through the project "3D printing, A bridge to the future (Grant 2017L7X3CS_004) within the PRIN 2017 program and by University of Rome Tor Vergata through the project "OPTYMA" (CUP E83C22002290005) within the "Ricerca Scientifica di Ateneo 2021" program. FAS acknowledges the funding by Fundação para a Ciência e a Tecnologia (FCT) in the framework of project UIDB/04625/2020.

The data that support the findings of this study are available from the corresponding author upon reasonable request.

REFERENCES

[1] P. Jiao, "Hierarchical metastructures with programmable stiffness and zero poisson's ratio," APL Materials **8**, 051109 (2020).
[2] S. Bonfanti, R. Guerra, M. Zaiser, and S. Zapperi, "Digital strategies for structured and architected materials design," APL Materials **9**, 020904 (2021).
[3] S. Shan, S. H. Kang, J. R. Raney, P. Wang, L. Fang, F. Candido, J. A. Lewis, and K. Bertoldi, "Multistable architected materials for trapping elastic strain energy," Adv. Mater. **27**, 4296–4301 (2015).
[4] J. R. Raney, N. Nadkarni, C. Daraio, D. M. Kochmann, J. A. Lewis, and K. Bertoldi, "Stable propagation of mechanical signals in soft media using stored elastic energy," Proceedings of the National Academy of Sciences **113**, 9722–9727 (2016).
[5] B. Deng, P. Wang, V. Tournat, and K. Bertoldi, "Nonlinear transition waves in free-standing bistable chains," Journal of the Mechanics and Physics of Solids **136**, 103661 (2020).
[6] J. Hua, H. Lei, C. F. Gao, X. Guo, and D. Fang, "Parameters analysis and optimization of a typical multistable mechanical metamaterial," Extreme Mech. Lett. **35**, 100640 (2020).
[7] H. Yang and L. Ma, "1D to 3D multi-stable architected materials with zero poisson's ratio and controllable thermal expansion," Mater. Des. **188**, 108430 (2020).
[8] R. Motro, *Tensegrity: structural systems for the future* (Kogan Page Science, London, U.K., 2003).
[9] R. E. Skelton and M. C. de Oliveira, *Tensegrity systems* (Springer, Boston, MA, US, 2009).
[10] R. Connelly and S. D. Guest, *Frameworks, Tensegrities, and Symmetry* (Cambridge University Press, 2022).
[11] I. J. Oppenheim and W. O. Williams, "Geometric effects in an elastic tensegrity structure," J. Elast. **59**, 51–65 (2000).
[12] I. J. Oppenheim and W. O. Williams, "Vibration of an elastic tensegrity structure," Eur. J. Mech. A/Solids **20**, 1023–1031 (2001).
[13] F. Fraternali, G. Carpentieri, and A. Amendola, "On the mechanical modeling of the extreme softening/stiffening response of axially loaded tensegrity prisms," J. Mech. Phys. Solids **74**, 136–157 (2015).
[14] I. J. Oppenheim and W. O. Williams, "Tensegrity prisms as adaptive structures," in *Proceedings of ASME International Mechanical Engineering Congress and Exposition: Adaptive Structures and Material Systems* (1997) pp. 113–120.
[15] K. Liu, J. Wu, G. H. Paulino, and H. J. Qi, "Programmable deployment of tensegrity structures by stimulus-responsive polymers," Sci. Rep. **7**, 3511 (2015).
[16] A. Amendola, A. Krushynska, C. Daraio, N. M. Pugno, and F. Fraternali, "Tuning frequency band gaps of tensegrity mass-spring chains with local and global prestress," Int. J. Solids Struct. **155**, 47–56 (2018).
[17] K. Pajunen, P. Celli, and C. Daraio, "Prestrain-induced bandgap tuning in 3d-printed tensegrity-inspired lattice structures," Extreme Mech. Lett. **44**, 101236 (2021).
[18] F. Fraternali, L. Senatore, and C. Daraio, "Solitary waves on tensegrity lattices," J. Mech. Phys. Solids **60**, 1137–1144 (2012).
[19] C. Daraio and F. Fraternali, "Method and apparatus for wave generation and

detection using tensegrity structures," U.S. Patent No. 8,616,328 (2013).

[20]F. Fraternali, G. Carpentieri, A. Amendola, R. E. Skelton, and V. F. Nesterenko, "Multiscale tunability of solitary wave dynamics in tensegrity metamaterials," Appl. Phys. Lett. **105**, 201903 (2014).

[21]C. Davini, A. Micheletti, and P. Podio-Guidugli, "On the impulsive dynamics of T3 tensegrity chains," Meccanica **51**, 2763–2776 (2016).

[22]A. Micheletti, G. Ruscica, and F. Fraternali, "On the compact wave dynamics of tensegrity beams in multiple dimensions," Nonlinear Dyn. **98**, 2737–2753 (2019).

[23]J. J. Rimoli and R. K. Pal, "Mechanical response of 3-dimensional tensegrity lattices," Compos. B. Eng. **115**, 30–42 (2017).

[24]A. Al Sabouni-Zawadzka and W. Gilewski, "Smart metamaterial based on the simplex tensegrity pattern," Materials **11** (2018), 10.3390/ma11050673.

[25]R. K. Pal, M. Ruzzene, and J. J. Rimoli, "Tunable wave propagation by varying prestrain in tensegrity-based periodic media," Extreme Mech. Lett. **22**, 149–156 (2018).

[26]D. De Tommasi, G. Puglisi, and F. Trentadue, "Elastic response of an optimal tensegrity-type metamaterial," Front. Mater. **6**, 24 (2019).

[27]F. A. Santos, "Towards a novel energy dissipation metamaterial with tensegrity architecture," Advanced Materials **n/a**, 2300639.

[28]K. Liu, T. Zegard, P. P. Pratapa, and G. H. Paulino, "Unraveling tensegrity tessellations for metamaterials with tunable stiffness and bandgaps," J. Mech. Phys. **131**, 147–166 (2019).

[29]K. Pajunen, P. Johanns, R. K. Pal, J. J. Rimoli, and C. Daraio, "Design and impact response of 3D-printable tensegrity-inspired structures," Mater. Des. **182**, 107966 (2019).

[30]C. Intrigila, A. Micheletti, N. A. Nodargi, E. Artioli, and P. Bisegna, "Fabrication and experimental characterization of a bistable tensegrity-like unit for lattice metamaterials," Addit. Manuf. , 102946 (2022).

[31]Z. Vangelatos, A. Micheletti, C. P. Grigoropoulos, and F. Fraternali, "Design and testing of bistable lattices with tensegrity architecture and nanoscale features fabricated by multiphoton lithography," Nanomaterials **10**, 652 (2020).

[32]J. Bauer, J. A. Kraus, C. Crook, J. J. Rimoli, and L. Valdevit, "Tensegrity metamaterials: toward failure-resistant engineering systems through delocalized deformation," Adv. Mater. **33**, 2005647 (2021).

[33]H. Y. Jeong, S.-C. An, and Y. C. Jun, "Light activation of 3D-printed structures: from millimeter to sub-micrometer scale," Nanophotonics **11**, 461–486 (2022).

[34]L.-Y. Hsu, P. Mainik, A. Münchinger, S. Lindenthal, T. Spratte, A. Welle, J. Zaumseil, C. Selhuber-Unkel, M. Wegener, and E. Blasco, "A facile approach for 4D microprinting of multi-photoresponsive actuators," Advanced Materials Technologies **8**, 2200801 (2023), https://onlinelibrary.wiley.com/doi/pdf/10.1002/admt.202200801.

[35]M. Defossez, "Shape memory effect in tensegrity structures," Mechanics Research Communications **30**, 311–316 (2003).

[36]A. Micheletti, "Bistable regimes in an elastic tensegrity system," Proc. R. Soc. A. **469**, 20130052 (2013).

[37]X. Xu and Y. Luo, "Multistable tensegrity structures," Journal of Structural Engineering **137(1)**, 117–123 (2010).

[38]S. D. Guest, "Understanding tensegrity with an energy function," in *Current Perspectives and New Directions in Mechanics, Modelling and Design of Structural Systems*, edited by A. Zingoni (CRC Press, 2022).

[39]S. D. Guest, "The stiffness of prestressed frameworks: A unifying approach," International Journal of Solids and Structures **43**, 842–854 (2006).

[40]S. D. Guest, "The stiffness of tensegrity structures," IMA Journal of Applied Mathematics **76**, 57–66 (2010).

[41]C. R. Calladine, "Buckminster Fuller's 'tensegrity' structures and Clerk Maxwell's rules for the construction of stiff frames," Int. J. Solids Struct. **14**, 161–172 (1978).

[42]C. R. Calladine and S. Pellegrino, "First-order infinitesimal mechanisms," Int. J. Solids Struct. **27**, 505–515 (1991).

[43]R. Connelly and W. Whiteley, "Second-order rigidity and prestress stability for tensegrity frameworks," SIAM J. Discrete Math. **9**, 453–491 (1996).

[44]R. Connelly, "Tensegrity structures: Why are they stable?" (2002) pp. 47–54.

[45]M. Schenk and S. D. Guest, "On zero stiffness," Proceedings of the Institution of Mechanical Engineers, Part C: Journal of Mechanical Engineering Science **228**, 1701–1714 (2014).

[46]A. Münchinger, V. Hahn, D. Beutel, S. Woska, J. Monti, C. Rockstuhl, E. Blasco, and M. Wegener, "Multi-photon 4D printing of complex liquid crystalline microstructures by in situ alignment using electric fields," Advanced Materials Technologies **7**, 2100944 (2022), https://onlinelibrary.wiley.com/doi/pdf/10.1002/admt.202100944.

[47]A. Münchinger, L.-Y. Hsu, F. Fürniß, E. Blasco, and M. Wegener, "3D optomechanical metamaterials," Materials Today **59**, 9–17 (2022).